Applied Catalysis A, General 652 (2023) 119034

Contents lists available at ScienceDirect

Applied Catalysis A, General

journal homepage: www.elsevier.com/locate/apcata

Effects of Cu_2O morphology on the performance of CO self-sustained catalytic combustion

Liangkai Wu [a,b,1], Pandong Ma [a,1], Chenhang Zhang [a,b], Xiaokun Yi [a], Qinglan Hao [a], Baojuan Dou [a,*], Feng Bin [b,*]

[a] Tianjin University of Science & Technology, Tianjin 300457, PR China
[b] State Key Laboratory of High-Temperature Gas Dynamics, Institute of Mechanics, Chinese Academy of Sciences, Beijing 100190, PR China

ARTICLE INFO

Keywords:
High-concentration carbon monoxide
Mechanism
Crystal plane
CO oxidation
Cu_2O

ABSTRACT

Self-sustained catalytic combustion is a sustainable approach to deal with exhaust gas with high concentration CO, and revealing its reaction process is necessary and challenging. Herein, cube (Cu_2O-C), octahedron (Cu_2O-O) and dodecahedron (Cu_2O-D) exposing different crystal planes were used to explore the catalytic combustion mechanism. The catalytic combustion can be self-sustained on the Cu_2O surface and the activities decrease in the order of Cu_2O-O > Cu_2O-D > Cu_2O-C, contributing to the different exposing planes with (1 1 1), (1 1 0) and (1 0 0), respectively. In-situ DRIFTS results prove that the catalytic combustion of CO to CO_2 on Cu_2O is prone to follow the MvK mechanism. Comparing with Cu_2O-D and Cu_2O-C, the relatively open surface of Cu_2O-O plane composed of unsaturated copper and oxygen atoms facilitates the CO adsorption on Cu (I) and the mobility of lattice oxygen, leading to the highest low temperature reducibility and catalytic activity.

1. Introduction

A large amount of non-recyclable converter exhaust gas with high concentration CO ($\leq$ 35%) is usually discharged into the atmosphere by combustion with methane, which consumes 1.3 million m^3 of methane every year in China, causing serious energy waste and environmental issues. To solve this problem, we developed a self-sustained catalytic combustion (SSCC) technology, which only relies on the heat released by CO continuously complete conversion to CO_2 over the catalyst, without external heat source. SSCC is flameless, which can avoid the explosion danger and NOx pollution, and the generated heat can be used for heating or power generation, except for maintaining its own oxidation reaction [1–4].

Copper based catalyst was proved to be an effective catalyst for SSCC of CO [2], and Cu (I) was discovered as the main active sites, which can provide 4 s1 empty orbit and a large number of binding sites for CO adsorption [3]. Furthermore, the activity of Cu (I) was usually influenced by the exposed crystal planes, hence selective exposure of highly active crystal planes is an effective strategy for optimizing the catalyst construction [5]. Cu_2O micro/nanocrystals were used for low concentration CO oxidation, and the morphology was found to influence the catalytic activity significantly with order of Cu_2O (1 1 1) > Cu_2O (1 1 0) > Cu_2O (1 0 0) [6,7]. However, compared with catalytic oxidation of low concentration CO, the SSCC of high concentration CO exhibits noticeable difference with three stages of induction step controlled by the intrinsic reaction kinetics, transient light-off step, and self-sustained combustion mainly depending on the diffusion [8]. Therefore, to explore the morphology effects of Cu_2O on SSCC of high concentration CO is of great important for better understanding the reaction mechanism with different stages.

In this paper, cubic Cu_2O-C, octahedral Cu_2O-O, and dodecahedral Cu_2O-D were prepared with the liquid-phase reduction method, and the catalytic performances were investigated through temperature programmed experiment of CO self-sustained catalytic combustion. The structure-activity relationships were deeply discussed combined with the results of SEM, TEM, XRD, XPS, H_2-TPR, N_2/CO/O_2-TPD-MS. And the reaction pathways on different crystal planes were analyzed based on the in-situ DRIFTS results.

* Corresponding authors.
E-mail addresses: bjdou@tust.edu.cn (B. Dou), binfeng@imech.ac.cn (F. Bin).
[1] These authors contributed to the work equally and should be regarded as co-first authors.

https://doi.org/10.1016/j.apcata.2023.119034
Received 5 October 2022; Received in revised form 7 December 2022; Accepted 9 January 2023
Available online 13 January 2023

2. Experimental

2.1. Catalyst preparation

Cu_2O micro/nanocrystals with different morphologies were prepared using liquid-phase reduction method [9]. For preparation of Cu_2O cube (Cu_2O-C) and octahedron (Cu_2O-O), 0.01 mol $CuCl_2{\cdot}2H_2O$ was dissolved in 1 L deionized water. In particular, 88.8 g Polyvinyl Pyrrolidone (PVP) as surface ligand was added into the solution for Cu_2O-O preparation. Then, the solution was mixed by magnetic stirring for 30 min at 55 ℃ followed by dropwise addition of 100 mL of NaOH solution (2 mol/L). After reacting at a constant temperature for 30 min, 100 mL ascorbic acid (0.6 mol/L) was added into the mixed solution with vigorous stirring at room temperature for 5 h (Cu_2O-C) and 3 h (Cu_2O-O), and bright red solid precipitate was gradually formed. Finally, the resulting precipitate was washed with deionized water until the solution was neutral, and dried at 60 ℃ for 12 h under vacuum.

For preparation of Cu_2O dodecahedron (Cu_2O-D), 0.01 mol $CuSO_4$ was dissolved in 400 mL deionized water. 40 mL oleic acid (surface ligand) and 200 mL ethanol which is used to dissolve oleic acid were mixed uniformly and added to the solution. The mixed solution was stirred for 30 min at 100 ℃ followed by adding 100 mL NaOH solution (0.8 mol/L) for another 5 min. Then, 34.2 g of glucose was dissolved in 300 mL deionized water, which was further added into the solution. The precursor solution was vigorous stirred for 1 h under the same temperature, and consequently obtained precipitate was further washed and dried in vacuum according to the above method.

2.2. Characterization

The morphology of catalysts was observed with a field-emission scanning electron microscope (SEM, ZEISS Gemini SEM 300) and transmission electron microscope (TEM, Philips Tecnai G2 F20). X-ray diffraction (XRD) measurements were tested with a Rigaku D/MAC/max 2500 v/pc diffractometer using the Cu Kα radiations (λ = 1.54059 Å) in the 2θ range with a scanning step size of 0.02° at room temperature. XRD data were processed and analyzed by JADE 6.0 software, compared with the standard cards derived from JCPDS files. The chemical state and composition on the surface of catalysts was analyzed by X-ray photoelectron spectroscopy (XPS) on a Thermo Scientific Escalab 250Xi using Mg Kα excitation. The C 1 S binding energy (284.8 eV) that arises from adventitious carbon was referenced to calibrate the binding energy. Temperature programmed reduction of hydrogen (H_2-TPR), temperature programmed desorption of carbon monoxide (CO-TPD) and temperature programmed desorption of oxygen (O_2-TPD) were conducted on a TP5080B Auto multifunctional adsorption instrument equipment. For H_2-TPR, 15 mg catalyst was pretreated at 300 ℃ for 30 min in N_2. After cooled to room temperature, swept with 5% H_2/Ar mixture (30 mL/min) until the baseline of the TCD signal unchanged. Finally, the sample was heated at a rate of 10 °C/min to record the TPR spectra. O_2-TPD and CO-TPD was carried out with the same pretreatment as H_2-TPR. Then, an O_2 or CO flow of 30 mL/min was switched to purge the simple for 30 min. Finally, the signal data was recorded at a heating rate of 15 °C/min. The in-situ DRIFTS spectroscopy was collected by a Nicolet 6700. Prior to recording the spectra, the sample were pretreated in N_2 at 300 °C for 60 min and was adsorbed in 25% CO/N_2 or 25% CO+ 25% O_2/N_2 for 30 min at room temperature. Then, the sample was heated to 400 °C at a rate of 10 °C/min.

2.3. Catalytic activity tests

The catalytic activity test was carried out in a fixed bed reactor [9]. 50 mg of catalyst mixed with 50 mg of quartz sand (100 mesh) were packed into a micro-reactor with an inner diameter of 6 mm. The sample was pretreated at 300 ℃ for 30 min in N_2 to eliminate impurities before introducing the mixed gas (10% CO, 21% O_2 and 69% N_2) with a flow rate of 200 mL/min (GHSV=60000 h^{-1}). Then, the sample was heated at a rate of 5 °C/min. A flue gas analyzer (Bruker Tensor 27 instrument) was used to monitor the effluent CO, and the CO conversion rate was obtained by calculating the average of the three experimental data. The stability test conditions are consistent with the above. After the CO conversion rate reached 100%, the heating was stopped and the heat source was provided by the reaction exothermic heat for 5 h.

3. Result and discussion

3.1. CO self-sustained catalytic combustion performance and durability

Prior to the activity test, the ligands on the surface of Cu_2O-O and Cu_2O-D were in situ removed by the controlled combustion [10]. The activity curves of CO self-sustained catalytic combustion in Fig. 1(a) for Cu_2O-C, Cu_2O-O and Cu_2O-D can be roughly divided into the three stages [2]. In the induction stage with CO conversion rate lower than 5%, the consumed CO and O_2 reactants can be quickly replenished through internal diffusion and the CO reaction rate is mainly controlled by the intrinsic reaction kinetics. With further increase temperature, the chemical heat released by the oxidation of high-concentration CO causes the instantaneous flying temperature reaching the critical temperature of CO ignition, and the CO spontaneously ignites at a higher temperature on the catalyst surface, with CO conversion rate close to 100%, and it is the second stage. In the third stage, the CO conversion rate of 100% no longer influenced by temperature changes, and the reaction mainly depends on the diffusion rate of the reactants to the catalyst surface, which is determined by the external diffusion and the catalytic activity.

T_{100} (the temperature corresponding to 100% CO conversion rate) of Cu_2O-O (1 1 1) is lowest (135 ℃) demonstrating the best activity, followed by Cu_2O-D (1 1 0) (145 ℃) and Cu_2O-C (1 0 0) (215 ℃). Fig. 1(b) shows the CO conversion rate and the temperature of catalyst bed for Cu_2O-C, Cu_2O-O and Cu_2O-D within 5 h under the self-sustained catalytic combustion at 193 ℃. It can be seen that, with no external heating, catalyst bed temperature did not decrease with 100% CO conversion rate, demonstrating that all the Cu_2O catalysts possess good thermal stability. The Arrhenius formula was used to calculate the apparent activation energy (Ea) of the three catalysts, as shown in Fig. 1(c). Lower Ea manifest easier catalytic reaction. Hence, the apparent activation energy of the three catalysts decreases in the order of Cu_2O-C (94.23 kJ/mol) > Cu_2O-D (77.54 kJ/mol) > Cu_2O-O (71.72 kJ/mol), which is consistent with the activity results in Fig. 1(a). Cu_2O-O exhibits the most excellent catalytic activity.

3.2. Morphology and structural characterizations

SEM and TEM in Fig. 2 shows that the morphologies of Cu_2O-C (a, d), Cu_2O-O (b, e) and Cu_2O-D (c, f) catalysts are very regular. Cu_2O-C is cubic exposing six (1 0 0) crystal planes [11], and octahedral Cu_2O-O exposes eight (1 1 1) crystal planes [12], and Cu_2O-D is dodecahedral exposing twelve (1 1 0) crystal planes [13]. It is worth noting that in the process of preparing Cu_2O-O, the amount of PVP added can influence the morphology of Cu_2O significantly. The selective interaction between the different crystal planes of PVP and Cu_2O reduces the growth rate of the crystal along the (1 1 1) direction, resulting in the formation of regular octahedrons with exposed (1 1 1) plane. If the amount of PVP is too low, the (1 1 1) plane cannot be completely covered, so the crystals exhibit irregular shapes [14]. Fig. 2(g) and Fig. 2(h) show the morphologies of Cu_2O-O with PVP addition of 44.4 g and 88.8 g respectively, indicating that proper amount of PVP is crucial for the formation of regular octahedron Cu_2O.

In Fig. 3, the XRD patterns of Cu_2O-C, Cu_2O-O and Cu_2O-D exhibit standard diffraction peaks of cubic phase Cu_2O (JCPDS 99–0041), and the peaks at 29.57°, 36.42°, 42.31°, 52.46°, 73.52° and 77.37° correspond to the (1 1 0), (1 1 1), (2 0 0), (2 1 1), (3 1 1) and (2 2 2) crystal planes of Cu_2O, respectively [11,15]. No diffraction peaks of other

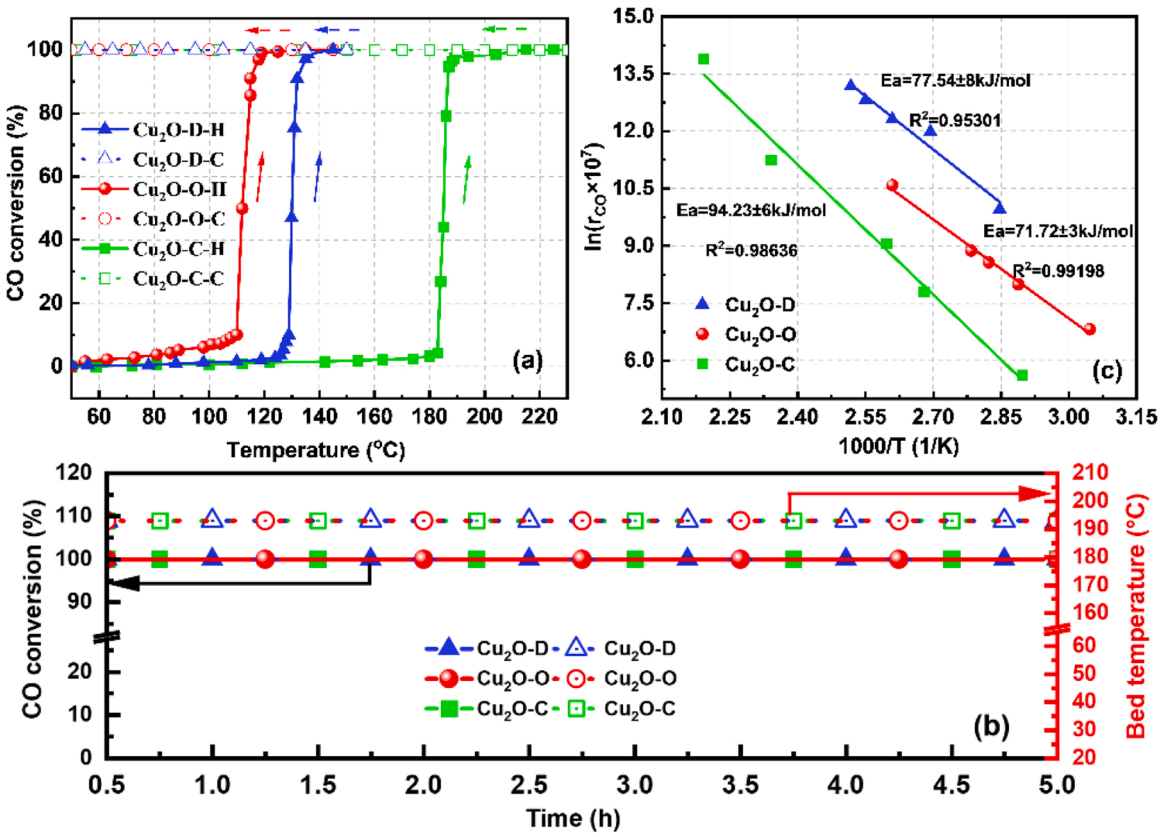

Fig. 1. (a) Activity curves, (b) thermal stability and (c) activation energy of CO self-sustained catalytic combustion over Cu_2O catalysts (H and C represent Heating and Cooling).

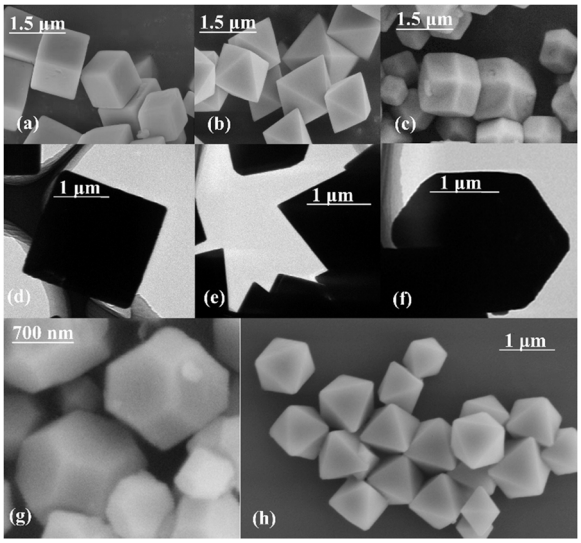

Fig. 2. SEM and TEM images of Cu_2O-C (a, d), Cu_2O-O (b, e), Cu_2O-D (c, f) and SEM images of Cu_2O-O with 44.4 g (g) or 88.8 g (h) PVP.

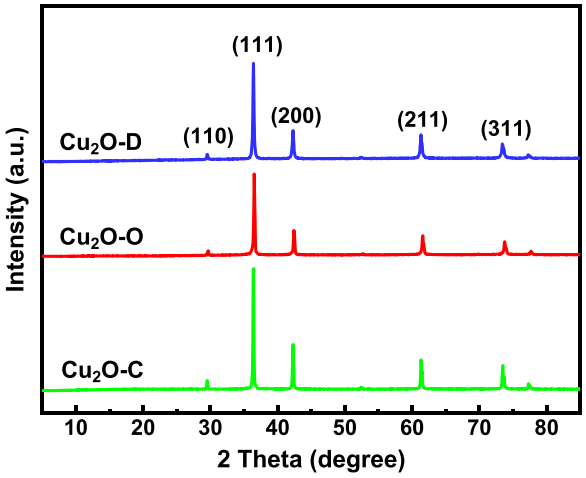

Fig. 3. XRD patterns of Cu_2O-C, Cu_2O-O and Cu_2O-D catalysts.

substances are founded in the XRD spectra of the three catalysts, and the sharp peaks correspond to the high purity and crystallinity of the prepared Cu_2O.

3.3. Chemical states

The full spectrum (Su), Cu 2p and O 1 s XPS spectra of the three catalysts are shown in Fig. 4, and the semi-quantitative analysis results of different elements are summarized in Table 1. From Fig. 4(a), all the catalysts exhibit characteristic diffraction peaks attributable to Cu 2p, O 1 s and C 1 s in the binding energy ranges of 962–928, 535–526 and 284.8 eV [10,13,16–18]. No obvious difference was detected for Cu 2p and O 1 s, while the intensities of C 1 s peaks decreases in the following order Cu_2O-D > Cu_2O-O > Cu_2O-C, relating to the surface ligands content on the surface of Cu_2O-O and Cu_2O-D. The surface ligands on the surface of Cu_2O-O and Cu_2O-D are PVP and oleic acid, respectively, and oleic acid is easier to adhere to the catalyst surface than PVP.

The binding energies of 530.5 eV, 531.5 eV and 532.5 eV in O 1 s XPS spectra (Fig. 4(b)) are attributable to lattice oxygen (O_L), oxygen in the OH^- (O_{OH}) and chemisorbed oxygen (O_C), respectively [19–21].

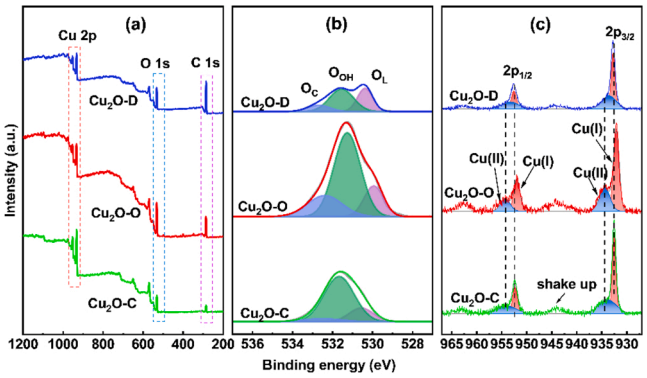

Fig. 4. XPS patterns of (a) Su, (b) O 1 s, and (c) Cu 2p for Cu_2O-C, Cu_2O-O and Cu_2O-D catalysts.

Since the obtained Cu_2O crystals grow in alkaline liquid, the oxygen species on the surface is mainly in the form of O_{OH}. The relative content of surface O_C decreases in the order of Cu_2O-O (20.5%) > Cu_2O-D (13.5%) > Cu_2O-C (6.5%), which is consistent with the order of catalytic activity. The increase of O_C on the catalyst surface demonstrates that Cu_2O-O can activate more gaseous oxygen and provides more active oxygen species to oxidize CO, lead to better activity. The peak intensity of Cu_2O-D is relatively lower , probably owing to the oleic acid covering the catalyst surface.

As indicated from the Cu 2p spectra in Fig. 4(c), the three catalysts are mainly existed in the form of Cu_2O. Among them, the peaks located near 932.5 eV and 952.3 eV are attributed to Cu (I), originated from Cu_2O. The peaks located around 933.8 eV and 954.1 eV can be assigned to Cu (II), due to the formation of $Cu(OH)_2$ in the alkaline liquid environment during the Cu_2O preparation. Cu (I) was proved as the active site controlling the CO oxidation to CO_2 over copper-based catalyst [3]. From Table 1, the Cu (I) content in Cu_2O-O is the highest, corresponding to the best catalytic activity of CO oxidation.

3.4. Redox properties

In general, the reducibility of catalysts is mainly related to the position of the low temperature reduction peak, and lower reduction temperature results in stronger reducibility of the catalyst. In Fig. 5, the reduction peaks in H_2-TPR curves of all the catalysts exhibit a certain asymmetry, which can be divided into two peaks α and β. The α increases in order of Cu_2O-O (209 ℃) < Cu_2O-D (213 ℃) < Cu_2O-C (250 ℃), consistent with the O_c in O 1 s XPS, indicating that the surface O_c can easily react with H_2 to form H_2O. The higher activity of coordinating unsaturated copper (Cu_{CUS}) and oxygen atoms (O_{CUS}) on the (1 1 1) plane results in better low temperature reducibility of Cu_2O-O. The β peak can be attributed to the reduction of Cu (I). Combining the activity evaluation results, it can be concluded that the catalytic activity of CO is positively correlated with the low temperature reducibility. The total H_2 consumption of Cu_2O-C is significantly larger than that of Cu_2O-O and Cu_2O-D (Table 1), probably owing to the actual mass of Cu_2O-O and Cu_2O-D is reduced after the in-situ removal of the surface ligands, compared with the same mass of Cu_2O-C.

Surface ligands were added to control the morphology in the process of preparing Cu_2O-O and Cu_2O-D. Part of the surface ligands between the catalyst crystal grains can be removed by cleanings with deionized water and ethanol, except for the surface ligands on the crystal surface. Therefore, a multi-gas adsorption-desorption mass spectrometer (M-TPD-MS) experiment was carried out to investigate the residual surface ligands. As shown Fig. S1, no CO_2 was detected before 300 ℃ in the N_2/CO/O_2-TPD-MS curves of Cu_2O-O and Cu_2O-D, owing to the pretreatment at 300 ℃ for 30 min. With increasing temperature higher than 300 ℃, two obvious CO_2 desorption peaks at 480 ℃ and 690 ℃ in Fig. S1 (a) was tracked attributing to the decomposition of PVP [11]. Fig. S1 (b) shows two obvious CO_2 desorption peaks at 480 ℃ and 610 ℃ owing to the decomposition of oleic acid [21–26]. Generally, in the absence of oxygen, CO will react with the lattice oxygen of the catalyst to form CO_2. However, the temperature and relative intensity of CO_2 peak from CO-TPD-MS exhibit no significant difference with O_2-TPD-MS and N_2-TPD-MS. Obviously, all CO_2 comes from the decomposition of the surface ligands and no additional CO_2 was produced. The result indicates that PVP and oleic acid form a dense protective film on the catalyst surface, which hinders the adsorption of CO and O_2.

3.5. In-situ DRIFTS study

The in-situ DRIFTS spectra of Cu_2O-D/O/C in Fig. 6 exhibit obvious CO absorption peaks at 2171 cm^{-1} and 2118 cm^{-1}, which are attributed to gas-phase CO and Cu^+-CO absorption peaks, respectively [8]. The peaks at 2340 cm^{-1} and 2360 cm^{-1} are assigned to the absorption peaks of gas phase CO_2 [27,28]. As depicted in Fig. 6(a), Cu^+-CO adsorbed on catalyst surface can be converted into CO_2 in the absence of oxygen, indicating that the CO_2 on the Cu_2O-D and Cu_2O-O is mainly produced by the reaction of Cu^+-CO with lattice oxygen, following the MvK

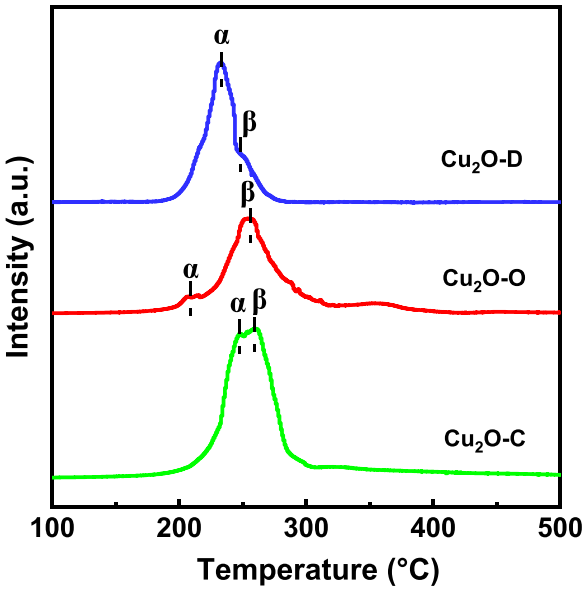

Fig. 5. H_2-TPR profiles of the Cu_2O-C, Cu_2O-O and Cu_2O-D catalysts.

Table 1
XPS semi-quantitative analysis and H_2 consumption of catalysts.

Catalyst	Surface atom percentage (%)					Reduction temperature (℃)		H_2 consumption (mmol/g)
	O/Cu	Cu^+/Cu	O_c/O	O_{OH}/O	O_L/O	α peak	β peak	Total
Cu_2O-D	28.0	50.2	13.5	52.5	44.0	213	235	2.15
Cu_2O-O	57.0	64.2	20.5	62.6	16.9	209	255	2.59
Cu_2O-C	36.3	51.4	6.5	75.3	18.2	250	260	4.50

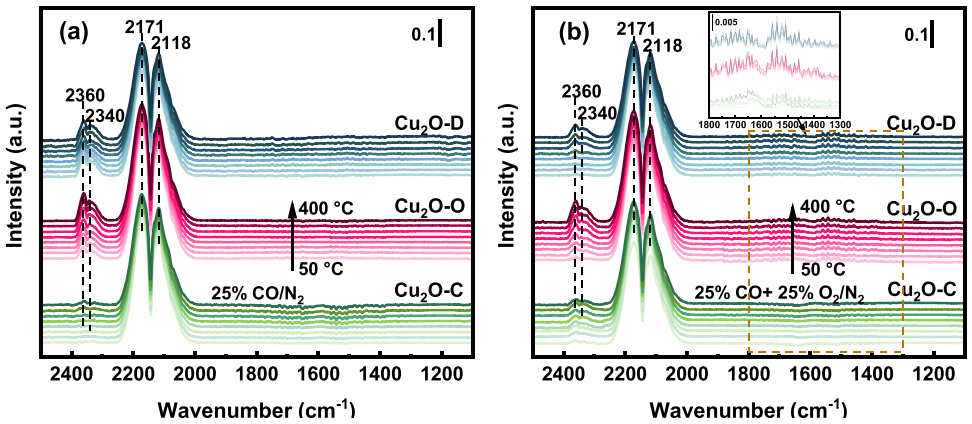

Fig. 6. In-situ DRIFT spectra of Cu_2O-D/O/C under (a) 25% CO/N_2 and (b) 25% CO+ 25% O_2/N_2.

mechanism. Relatively small amount of lattice oxygen of Cu_2O-C is consumed higher than 350 °C to generate a weak CO_2 absorption peak, while Cu_2O-D and Cu_2O-O can generate a strong CO_2 absorption peak at low temperature. With the increase of temperature, the CO_2 absorption peak intensity of Cu_2O-D gradually decreases, while that of Cu_2O-O continues to increase, which further demonstrates that the transfer ability of lattice oxygen in Cu_2O-O is stronger than that in Cu_2O-C and Cu_2O-D. After the introduction of gaseous oxygen (Fig. 6b), oxygen can be continuously supplemented into the oxygen vacancies, which promotes the rapid generation and desorption of CO_2. Compared with the spectra with no O_2 (Fig. 6a), new absorption peaks in the range of 1300–1800 cm^{-1} are observed in the presence of gaseous O_2, attributing to the bridge carbonate formed by CO adsorption on O atoms [29]. Combined with Fig. 6(a) and (b), it can be inferred that, in the presence of gaseous oxygen, a very small fraction of CO adsorbed on the three catalysts is oxidized to CO_2 in the form of carbonate, which is consistent with the L-H mechanism. Therefore, the catalytic combustion reaction of CO on Cu_2O-D, Cu_2O-C and Cu_2O-O mainly follows the MvK mechanism, with a small part following the L-H mechanism.

3.6. Structure-activity relationship and reaction pathway

According to the results of XRD, SEM and TEM, cubic Cu_2O-C, octahedral Cu_2O-O and dodecahedral Cu_2O-D with high crystallinity and regular morphology expose (1 0 0), (1 1 1) and (1 1 0) planes, respectively. Based on the CO-TPO results, the activity of different crystal planes of Cu_2O decreases in order of (1 1 1) > (1 1 0) > (1 0 0). In-situ DRIFTS results confirms that CO catalytic combustion over Cu_2O catalysts primarily follows the MvK mechanism. CO is first adsorbed on Cu (I) (step 1 in Fig. 7), and then the adjacent active lattice oxygen attacks CO to generate CO_2 forming oxygen vacancies (step 2). Finally, gaseous oxygen is supplemented to the oxygen vacancies to complete a cycle (step 3). And the CO adsorption is the rate-controlling step for the whole oxidation reaction, which will significantly influence the activity of the catalyst [3].

As shown in Fig. 7, the surface atomic arrangement is related to the ability of CO adsorption on Cu_2O surface and the catalytic activity. The outermost layer of the (1 0 0) crystal plane for Cu_2O-C is entirely composed of O_{CUS}, and the second layer consists of coordination saturated copper (Cu_{CSA}). Due to the compact surface and the absence of active copper sites in the outermost layer, CO is hardly chemisorbed on (1 0 0) [6]. For (1 1 0), the outermost layer is composed of both O_{CUS} and Cu_{CSA}, and the second layer is composed of Cu_{CSA}, which is favorable to CO adsorption on the active copper sites. With regard to (1 1 1), the outermost layer is formed of O_{CUS}, and the second layer has Cu_{CUS} (Cu_{CSA}: Cu_{CUS}=3:1) which allow stronger accessibility for CO than Cu_{CSA}. Although there are no active copper sites in the outermost layers of the (1 1 1), the surface of (1 1 1) crystal plane is very open, and the coordinately unsaturated copper atoms in the second layer can easily interact with CO. Therefore, the Cu_2O-O catalyst with the exposed (1 1 1) crystal plane exhibits the best CO catalytic activity.

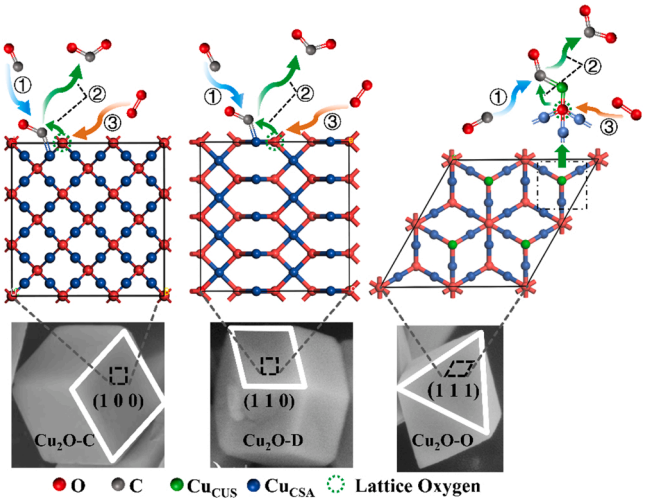

Fig. 7. Reaction pathway of CO catalytic combustion on different crystal planes of Cu_2O.

From the analysis of XPS results, it is known that Cu_2O-O exhibits the most O_C content with the order of Cu_2O-O (20.5%) > Cu_2O-D (13.5%) > Cu_2O-C (6.5%), which is consistent with the order of catalytic activity. This can be explained by the more active Cu_{CUS} and O_{CUS} on the (1 1 1) plane, consequently enhancing the mobility of oxygen in the reaction. In contrast, the lowest O_C content is detected on Cu_2O-C surface, which is associated with its (1 0 0) crystal plane terminated by O and followed by Cu_{CSA}. As indicated by H_2-TPR, Cu_2O-O possesses the best low temperature reducibility. Therefore, the unique atomic arrangement and the strongly reactive Cu_{CUS} atom of (1 1 1) crystal plane make Cu_2O-O exhibits the best CO catalytic activity.

4. Conclusion

In this paper, cubic (1 0 0), octahedral (1 1 1) and dodecahedral (1 1 0) Cu_2O micro/nanocrystalline catalysts were employed to investigate the effect of crystal planes on the performance of self-sustained catalytic combustion reaction for high concentration CO. It was found that the catalytic activity is positively correlated with the low temperature reducibility, and decrease in the order of Cu_2O-O > Cu_2O-D > Cu_2O-C. Compared with the (1 0 0) and (1 1 0) planes, the open surface structure and the strongly reactive Cu_{CUS} and O_{CUS} atoms of the (1 1 1) plane

enhance the CO adsorption and ability to activate gaseous oxygen, thereby promoting the conversion of CO to CO_2. In-situ DRIFTS experiments proved that the catalytic combustion reaction of CO on Cu_2O-D, Cu_2O-C and Cu_2O-O catalysts mainly follows the MvK mechanism, with a small part following the L-H mechanism.

CRediT authorship contribution statement

Liangkai Wu: performed the experiments, the data analyses and wrote the manuscript. **Pandong Ma:** contributed to the conception of the study; performed the experiments. **Chenhang Zhang:** performed the experiments. **Xiaokun Yi:** collected the data. **Qinglan Hao:** verified the data. **Baojuan Dou:** contributed significantly to analysis and manuscript preparation. **Feng Bin:** helped perform the analysis with constructive discussions.

Declaration of Competing Interest

The authors declare that they have no known competing financial interests or personal relationships that could have appeared to influence the work reported in this paper.

Data Availability

The authors are unable or have chosen not to specify which data has been used.

Acknowledgements

This work was supported by the Novel Technology of High Efficient Clean Combustion and Energy Saving on Converter Gas (XDA21040500) and the National Natural Science Foundation of China (No. 52176141).

Appendix A. Supporting information

Supplementary data associated with this article can be found in the online version at doi:10.1016/j.apcata.2023.119034.

References

[1] F. Bin, X. Wei, B. Li, K.S. Hui, Appl. Catal. B 162 (2015) 282–288.
[2] F. Bin, R. Kang, X. Wei, Q. Hao, B. Dou, Proc. Combust. Inst. 37 (2019) 5507–5515.
[3] R. Kang, X. Wei, F. Bin, Z. Wang, Q. Hao, B. Dou, Appl. Catal. A Gen. 565 (2018) 46–58.
[4] R. Kang, X. Wei, P. Ma, F. Bin, J. He, Q. Hao, B. Dou, Fuel 263 (2020).
[5] Y.Y. Song, B. Dong, S.W. Wang, Z.R. Wang, M. Zhang, P. Tian, G.C. Wang, Z. Zhao, ACS Omega 5 (2020) 6260–6269.
[6] Q. Hua, T. Cao, H. Bao, Z. Jiang, W. Huang, ChemSusChem 6 (2013) 1966–1972.
[7] H. Bao, W. Zhang, D. Shang, Q. Hua, Y. Ma, Z. Jiang, J. Yang, W. Huang, J. Phys. Chem. C. 114 (2010) 6676–6680.
[8] Z. Teng, J. Yun, L. Du, J. Huang, Q. Hao, B. Dou, K.N. Hui, F. Bin, N. J. Chem. 45 (2021) 20629–20640.
[9] P. Ma, Z. Teng, Q. Hao, R. Kang, B. Li, F. Bin, B. Dou, Fuel 289 (2021).
[10] Hua Q., 2012. Doctoral thesis, University of Science and Technology of China (2012). [in Chinese].
[11] D. Tang, J. Hu, Y. Zhang, C. Hu, Acta Chim. Sin. 68 (2010) 1379–1384.
[12] Jiao C., Master's thesis, Guilin University of Technology (2018). [in Chinese].
[13] W.C.J. Ho, Q. Tay, H. Qi, Z. Huang, J. Li, Z. Chen, Molecules 22 (2017).
[14] X. Zhang, Y. Xie, F. Xu, X. Liu, D. Xu, Inorg. Chem. Commun. 6 (2003) 1390–1392.
[15] B. Liu, X. Yao, Z. Zhang, C. Li, J. Zhang, P. Wang, J. Zhao, Y. Guo, J. Sun, C. Zhao, ACS Appl. Mater. Interfaces 13 (2021) 39165–39177.
[16] Y. Wang, J. Yun, L. Zhu, B. Cao, J. Gao, X. Shi, Y. Huang, P. Liu, G. Zhu, Appl. Surf. Sci. 603 (2022), 154469.
[17] J. Li, L. Huang, Z. Yang, Z. Liu, X. Sun, J. Environ. Chem. Eng. 10 (2022).
[18] X.L. Luo, Y.F. Han, D.S. Yang, Y.S. Chen, Wuli Huaxue Xuebao/ Acta Phys. - Chim. Sin. 28 (2012) 297–302.
[19] W.T. Wu, L. Shi, Q. Zhu, Y. Wang, G. Xu, W. Pang, F. Lu, Chem. Lett. 35 (2006) 574–575.
[20] S. Sun, D. Deng, C. Kong, Y. Gao, S. Yang, X. Song, B. Ding, Z. Yang, CrystEngComm 13 (2011) 5993–5997.
[21] L. Gou, C.J. Murphy, Nano Lett. 3 (2003) 231–234.
[22] Wei X., 2017. Master's thesis, Zhejiang Sci-Tech University (2017). [in Chinese].
[23] Fu L., 2013. Master's thesis, Jilin University (2013). [in Chinese].
[24] Jia W., 2015. Doctoral thesis, Tsinghua University (2015). [in Chinese].
[25] Xu X., 2015. Master's thesis, Tianjin University (2015). [in Chinese].
[26] Zhang L., 2015. Doctoral thesis, China University of Mining and Technology (2015). [in Chinese].
[27] Y. Gao, Z. Zhang, Z. Li, W. Huang, Chin. J. Catal. 41 (2020) 1006–1016.
[28] W.W. Wang, W.Z. Yu, P.P. Du, H. Xu, Z. Jin, R. Si, C. Ma, S. Shi, C.J. Jia, C.H. Yan, ACS Catal. 7 (2017) 1313–1329.
[29] Q. Hua, T. Cao, X.K. Gu, J. Lu, Z. Jiang, X. Pan, L. Luo, W.X. Li, W. Huang, Angew. Chem. - Int. Ed. 53 (2014) 4856–4861.